iScience

CellPress

Article

A Bifunctional Fluorophosphate Electrolyte for Safer Sodium-Ion Batteries

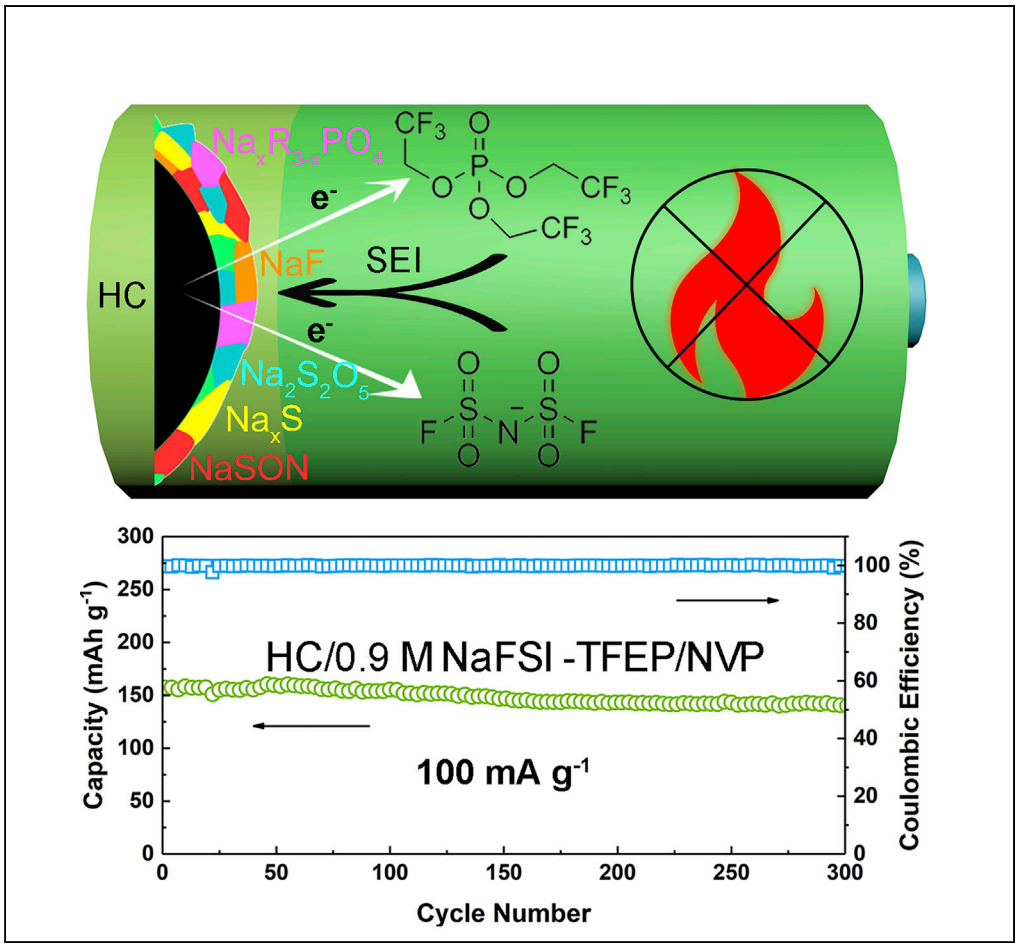

Xiaoyu Jiang, Xingwei Liu, Ziqi Zeng, Lifen Xiao, Xinping Ai, Hanxi Yang, Yuliang Cao

ylcao@whu.edu.cn

HIGHLIGHTS

A novel bifunctional TFEP electrolyte is designed for safe SIBs

The nonflammable TFEP electrolyte shows high electrochemical stability

TFEP solvent can participate in SEI formation at HC anode surface

The HC/NVP cell in TFEP electrolyte delivers high capacity with long working life

Jiang et al., iScience *10*, 114–122
December 21, 2018
https://doi.org/10.1016/j.isci.2018.11.020

iScience

CellPress

Article

A Bifunctional Fluorophosphate Electrolyte for Safer Sodium-Ion Batteries

Xiaoyu Jiang,[1] Xingwei Liu,[1] Ziqi Zeng,[1] Lifen Xiao,[2] Xinping Ai,[1] Hanxi Yang,[1] and Yuliang Cao[1,3,*]

SUMMARY

Most of the currently developed sodium-ion batteries (SIBs) have potential safety hazards due to the use of highly volatile and flammable alkyl carbonate electrolytes. To overcome this challenge, we report an electrochemically compatible and nonflammable electrolyte, tris(2,2,2-trifluoroethyl) phosphate (TFEP) with low-concentration sodium bis(fluorosulfonyl)imide (0.9 M), which is designed not only to match perfectly with the hard carbon (HC) anode but also to enhance the thermal stability of SIBs. Experimental results and theoretical calculations reveal that TFEP molecules have a significantly low barrier to decompose before Na^+ inserts into HC, forming a stable inorganic solid-electrolyte interface layer, thus improving the electrochemical and structural stabilities of HC anodes. An HC/$Na_3V_2(PO_4)_3$ full cell using TFEP electrolyte shows a high capacity retention of 89.2% after 300 cycles and a dramatically reduced exothermic heat at elevated temperature, implying its potential application for safe and low-cost larger-scale energy storage.

INTRODUCTION

Sodium-ion batteries (SIBs) are now proposed as a potential large-scale energy storage technology because of the low cost and high abundance of sodium resources (Fang et al., 2017; Wu et al., 2017; Bella et al., 2017, 2018). As an indispensable constituent of SIBs, the electrolyte plays a key role in determining the electrochemical performance and safety of the batteries. However, the most commonly used electrolytes for SIBs are still based on alkyl carbonate solvents, which are volatile and flammable, imposing a potential safety hazard for large-scale applications (Xia et al., 2017; Bommier and Ji, 2018). On the other hand, the alkyl carbonates often form an organic-rich solid-electrolyte interface (SEI) layer on the anode during the initial charge (Qi et al., 2017; Eshetu et al., 2016; Xu, 2014). These organic Na compounds in SEI have a much higher solubility than their Li counterparts because of the lower Lewis acidity of Na (Iermakova et al., 2015; Mogensen et al., 2016; Westman et al., 2018), leading to continuous electrolyte depletion and, therefore, inferior cyclability. Consequently, it is necessary to develop novel electrolyte systems with high safety and surface passivation capabilities.

To improve the safety of batteries by avoiding leakage of the flammable electrolytes and reducing gas production in abuse condition, the most straightforward approach is to apply the gel polymer electrolyte (GPE), which is composed of a polymeric framework and a certain amount of liquid electrolyte (Che et al., 2017; Feuillade and Perche, 1975; Zheng et al., 2018). For instance, the $LiNi_{0.8}Co_{0.15}Al_{0.05}O_2$ (NCA)/graphite-Si/C pouch battery using poly(pentaerythritol tetraacrylate) GPE cannot combust in the puncture experiment, whereas the battery using liquid carbonate electrolyte underwent a violent combustion (Li et al., 2017). Other good examples of GPEs are poly(ethylene oxide) (Colò et al., 2017), polyvinylpyrrolidone (Rao et al., 2019), poly(ethylene glycol) methyl ether methacrylate (Bella et al., 2015), poly(vinylidene fluoride-co-hexafluoropropylene) (Kim et al., 2017), and poly(ethylene glycol) divinyl ether-co-bisphenol ethoxylate dimethacrylate (Zhang et al., 2017). Although the GPE can alleviate some safety hazards such as liquid leaking and combustion in battery systems, the reaction between the charged electrode and liquid electrolyte at elevated temperature is still an issue.

Alkyl phosphates exhibit similar physicochemical properties, e.g., high dielectric permittivity and low viscosity, as alkyl carbonates but are intrinsically nonflammable (Xu et al., 2002; Feng et al., 2008). In addition, alkyl phosphates are less reactive to charged electrodes at elevated temperatures (Jiang et al., 2017; Matsumoto et al., 2015), further improving the safety of the batteries. Thus, utilizing alkyl phosphates as electrolyte solvents may resolve the thermal safety problems of batteries. Previous works have proved that trimethyl phosphate- and triethyl phosphate (TEP)-based electrolytes have good compatibility with conventional electrode materials, including $NaNi_{0.35}Mn_{0.35}Fe_{0.3}O_2$, S_8, SiO, and Sb (Zeng et al.,

[1]College of Chemistry and Molecular Sciences, Hubei Key Laboratory of Electrochemical Power Sources, Wuhan University, Wuhan 430072, China

[2]State Key Laboratory of Advanced Technology for Materials Synthesis and Processing, Wuhan University of Technology, Wuhan 430070, China

[3]Lead Contact

*Correspondence: ylcao@whu.edu.cn

https://doi.org/10.1016/j.isci.2018.11.020

2016; Matsumoto et al., 2015; Yang et al., 2018). Unfortunately, these alkyl phosphate electrolytes are electrochemically incompatible with carbonaceous materials, which are widely used as high-capacity, low-cost anodes of SIBs, because their decomposition products on carbon anodes are unable to form a compact SEI layer (Xu et al., 2003). This issue can be alleviated using highly concentrated electrolytes (commonly >3 mol L^{-1}). Recent studies reveal that increasing the salt concentration results in the formation of a three-dimensional solution structure without free solvent molecules, effectively suppressing the reactivity of the electrolyte solvent (Wang et al., 2018; Zeng et al., 2018; He et al., 2016; Liu et al., 2018b). In addition, some special anions (FSI^- or $TFSI^-$) in the high-concentration electrolyte preferentially decompose to form a robust and compact SEI film on the carbon anode, which further inhibits the side reaction of the electrolyte (Sogawa et al., 2017; Yamada et al., 2014; Jiang et al., 2018; Patra et al., 2019). Despite its good compatibility with the carbon anode, high-concentration electrolytes also have several drawbacks, such as requiring large amounts of expensive salts, poor wettability, and high viscosity, which hinder their commercialization process (Yamada and Yamada, 2015).

Rather than using a highly concentrated electrolyte, we present here another feasible strategy to stabilize the phosphate electrolyte on carbonaceous electrodes by introducing fluorine atoms into the molecules. Owing to the strong electronegativity of the F atom, fluoroalkyl phosphate shows poorer resistance to the reduction reaction than alkyl phosphate and should decompose before Na^+ inserts into the carbon anode to form a stable SEI film, thus avoiding repeated SEI formation/damage (Zhao et al., 2017; Xiang et al., 2018; Song et al., 2018; Xu et al., 2016). Such a compact and dense SEI film on carbonaceous anodes can improve the electrochemical performance of hard carbon (HC) anodes. Therefore, a normal concentration (~1 M) rather than a highly concentrated electrolyte (>3 M) would be used to suppress the decomposition of solvent, greatly reducing the electrolyte cost to meet commercial requirements. In addition, the thermally stable inorganic SEI layer (e.g., NaF) originating from the decomposition of fluorophosphate can reduce reactivity between the sodiated anode and electrolyte at elevated temperatures, leading to extraordinary thermal safety for the SIB (Liu et al., 2018a; Zhao et al., 2013). Moreover, partial fluorine substitution creates a synergistic flame-retardant effect to further reduce the possibility of battery combustion. As a proof of concept, we demonstrate for the first time a highly safe, high-performance SIB with an HC anode, a $Na_3V_2(PO_4)_3$ (NVP) cathode, and a novel bifunctional electrolyte composed of tris(2,2,2-trifluoroethyl) phosphate (TFEP) solvent and low-concentration NaFSI (0.9 M).

RESULTS AND DISCUSSION

Physicochemical Properties of the TFEP-Based Electrolytes

The chemical stability of TFEP toward Na is visually examined by storing Na pieces in the TFEP solvent. As shown in Figure 1A, even after 9 months of storage at room temperature, the surface of the Na metal remains bright, indicating high chemical stability of TFEP with Na. In contrast, the fluorine-free phosphate, TEP, reacted with Na and slowly generated bubbles (Figure S1). After 7 days, the Na metal was largely consumed, and the solution turned into a yellowish gel (Figure 1B). This difference can be ascribed to the stability of different SEI layers. According to density functional theory with the B3LYP/6-311G basis set, TFEP has a relatively high electron affinity (low lowest unoccupied molecular orbital [LUMO] energy level), which facilitates the generation of a dense protective layer (mainly NaF) on the surface of Na via preferred reductive decomposition, suppressing the subsequent corrosion of Na (Figure 1C) (Okuno et al., 2016; Lee et al., 2018). Conversely, in a TEP solution, the TEP-derived SEI shows higher solubility, resulting in the continuous corrosion of Na. Therefore, TFEP can be used to build a highly stable SIB because of its low LUMO energy level and excellent anodic passivation ability. The non-flammability of TFEP was examined by an igniting test. TFEP could not be ignited completely (Figure 1E), whereas the carbonate solvent of a mixture of ethylene carbonate (EC) and diethyl carbonate (DEC) (1:1, V/V) started a fire rapidly after ignition (Figure 1D). Apparently, use of the TFEP electrolyte can remarkably enhance SIB safety.

Figure S2 displays the room temperature ionic conductivities of TFEP electrolytes with various NaFSI contents. The electrolyte containing 0.9 M NaFSI displays the highest conductivity of 0.43 mS cm^{-1}. In this regard, 0.9 M NaFSI-TFEP electrolyte was used in subsequent electrochemical investigations. The electrochemical window of the 0.9 M NaFSI-TFEP electrolyte was evaluated by cyclic voltammetry (CV) on a Pt microelectrode (Figure S3). The CV curve shows no additional redox peaks in a potential range of 0–5.0 V (versus Na/Na^+) aside from a couple of highly reversible Na deposition/dissolution peaks observed, demonstrating a wide window of electrochemical stability.

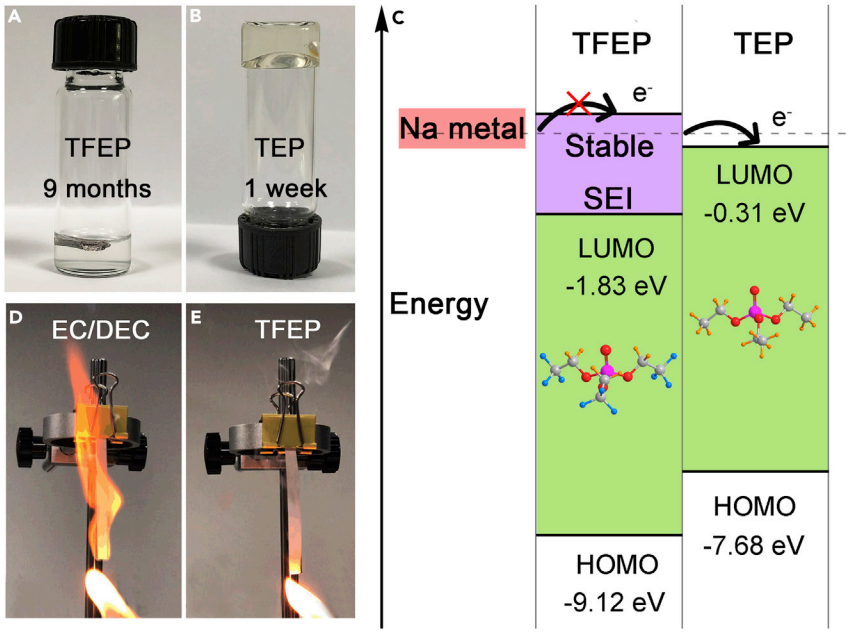

Figure 1. Comparison of TFEP and Carbonate Electrolytes in Terms of Chemical Stability and Flammability

(A and B) Images of Na metal stored in TFEP (A) and TEP (B).

(C) Energy level diagrams of TFEP and TEP. HOMO, highest occupied molecular orbital.

(D and E) Ignition test of EC/DEC (D) and TFEP solvent (E).

See also Figure S1.

Electrochemical Performance of Hard Carbon Anode in 0.9 M NaFSI-TFEP Electrolyte

The electrochemical performance of the HC anode in 0.9 M NaFSI-TFEP electrolyte is shown in Figure 2. The initial CV curve shows a broad cathodic peak from 1.0 to 0.4 V and a pair of redox peaks at approximately 0.1 V (Figure 2A), corresponding to the formation of an SEI layer and Na^+ insertion/extraction into/from the carbon layers, respectively (Qiu et al., 2017; Xiao et al., 2018). The initial galvanostatic charge-discharge profile of the HC anode exhibits a sloping region above 0.2 V and a plateau region at approximately 0.1 V (Figure 2B), which is consistent with the CV results. The HC anode in the 0.9 M NaFSI-TFEP electrolyte can deliver an initial reversible capacity of 239 mAh g^{-1} with an initial coulombic efficiency (ICE) of 75.4% at 20 mA g^{-1}, which is similar to those in a 1 M $NaClO_4$-EC/DEC electrolyte of 264 mAh g^{-1} and 74.1%, respectively (Figure S4A). In addition, the HC anode in TFEP electrolyte exhibits a stable cyclic behavior with a capacity retention of 91.8% for 100 cycles at 50 mA g^{-1} and a coulombic efficiency (CE) of nearly 100% throughout cycling (Figure 2C). The rate performance of the HC anode in a 0.9 M NaFSI-TFEP electrolyte is shown in Figure 2D. Reversible capacities of 238, 210, 165, 84.0, 46.5, and 25.2 mAh g^{-1} are presented at 20, 50, 100, 200, 500, and 1,000 mA g^{-1}, respectively, which are slightly lower than those in 1 M $NaClO_4$-EC/DEC (Figure S4B) due to the relatively lower ionic conductivity of the TFEP-based electrolyte. When the current density returns to 50 mA g^{-1}, the HC anode can fully recover its original reversible capacity value in the TFEP-based electrolyte (Figure 2D). Overall, the HC anode using a 0.9 M NaFSI-TFEP electrolyte displays a high capacity, an excellent cycling stability, and a good rate capability and is fully capable for battery applications.

Characterization of the SEI Layer on HC Anode

The excellent electrochemical performances of HC in TFEP-based electrolyte should be ascribed to the formation of a dense and compact SEI layer on the HC surface. To identify the morphology and composition of the SEI layer, scanning electron microscopy, transmission electron microscopy (TEM), and X-ray photoelectron spectroscopy (XPS) were conducted on an HC anode cycled in a 0.9 M NaFSI-TFEP electrolyte for 10 times. The surface morphology of the cycled HC anode (Figure 3A) remains nearly the same as that of the original HC anode (Figure S5), indicating that the SEI layer is uniform, dense, and extremely thin. This deduction is supported by the TEM image (Figure 3B), which depicts a dense and well-adhered SEI layer ca. 20 nm thick. Figures 3C–3F show the F 1s, P 2p, S 2p, and N 1s spectra of the cycled HC anode.

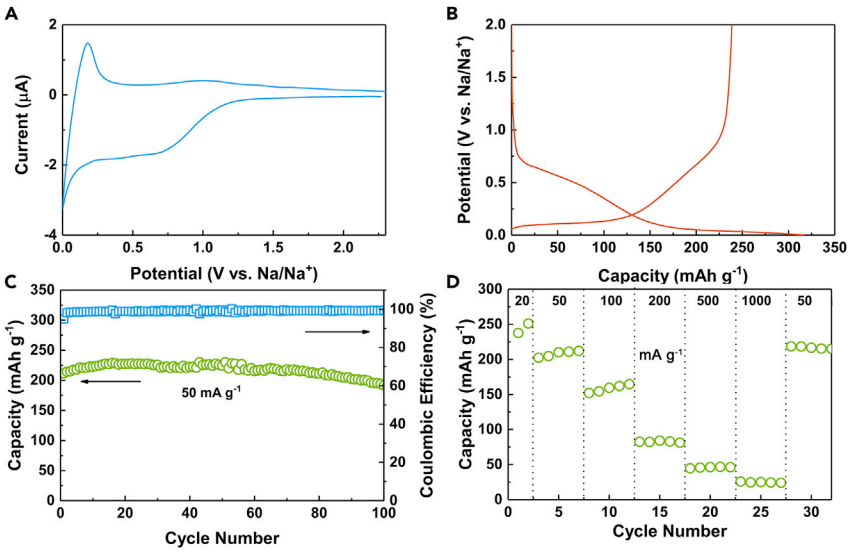

Figure 2. Electrochemical Performances of HC Anodes in a 0.9 M NaFSI-TFEP Electrolyte

(A) Initial CV curve at 0.1 mV s^{-1}.

(B) Initial charge/discharge profile at 20 mA g^{-1}.

(C) Cycling performance at 50 mA g^{-1}.

(D) Rate capability.

See also Figures S3 and S4.

The existence of NaF (684.3 eV) and PO_4^{3-} (133.7 eV) may derive from the decomposition of the TFEP solvent. This speculation is further verified by the XPS spectra of the HC anode cycled in a $NaClO_4$-TFEP electrolyte with non-fluorinated salt (Figure S6B). Without the F-contained salt, the characteristic peak of NaF is still observed, which can only derive from the decomposition of TFEP solvent. Besides, the Na/HC cell in $NaClO_4$-TFEP electrolyte displays a conventional charge-discharge curve but delivers a lower reversible capacity of 200 mAh g^{-1} (Figure S6A). The inferior electrochemical performance is ascribed to the very low Na^+ conductive ability (0.06 mS cm^{-1}) of $NaClO_4$-TFEP electrolyte and thus induces higher polarization. In addition, residual FSI^- (S-F at 168.8 eV, -SON at 398.4 eV) and its degradation products (NaF, $Na_2S_2O_5$, S, Na_xS, Na_2S, and NaSNO at 399.7 eV) are detected as well (Wang et al., 2018; Kim et al., 2015; Philippe et al., 2013). All these inorganic species form a compact and robust SEI layer to synergistically suppress the electrochemical reduction of the TFEP solvent on the HC anode surface (Figure 3G). According to the above discussion, it can be supposed that the preferred reducible TFEP solvent can easily produce inorganic NaF via a two-electron reduction step (Figure 3H), which constructs a stable interface to facilitate sodium-ion insertion/extraction into/from the HC anode (Shinichi et al., 2011; Komaba et al., 2011).

Electrochemical Performance of HC/$Na_3V_2(PO_4)_3$ Battery with 0.9 M NaFSI-TFEP

To verify the potential application of the TFEP-based electrolyte for a full cell, we selected a carbon-coated NVP composite as the cathode material to pair with the HC anode. As shown in Figure S7A, the NVP cathode in TFEP-based electrolyte delivers an initial reversible capacity of 110.3 mAh g^{-1} and a CE of 99.9% at 24 mA g^{-1}, which are similar to those delivered by one using conventional carbonate electrolyte. The higher polarization during charge-discharge process of NVP cathode in the TFEP-based electrolyte is ascribed to the lower ionic conductivity of the TFEP electrolyte. However, the NVP cathode shows comparable rate capability with that using conventional electrolyte (Figure S7B). Owing to the intrinsic structural stability and high Na^+ ion conductivity of NVP, the Na/NVP half-cell using the 0.9 M NaFSI-TFEP electrolyte can deliver a high rate capacity of 87 mAh g^{-1} at 1,170 mA g^{-1} (10 C) and exhibits a capacity retention of 83.5% after 10,000 cycles (Figure S7C), displaying an extremely long cycling life. Subsequently, the charge/discharge performance of an HC/NVP full cell using a 0.9 M NaFSI-TFEP electrolyte was evaluated. As shown in Figure 4A, the full cell delivers an initial discharge capacity of 221.5 mAh g^{-1} at 20 mA g^{-1} (based on the mass of HC anode) with an average operating voltage of 3.26 V and an ICE of 70.6%. In addition, rate discharge capacities of 219.2, 195.9,

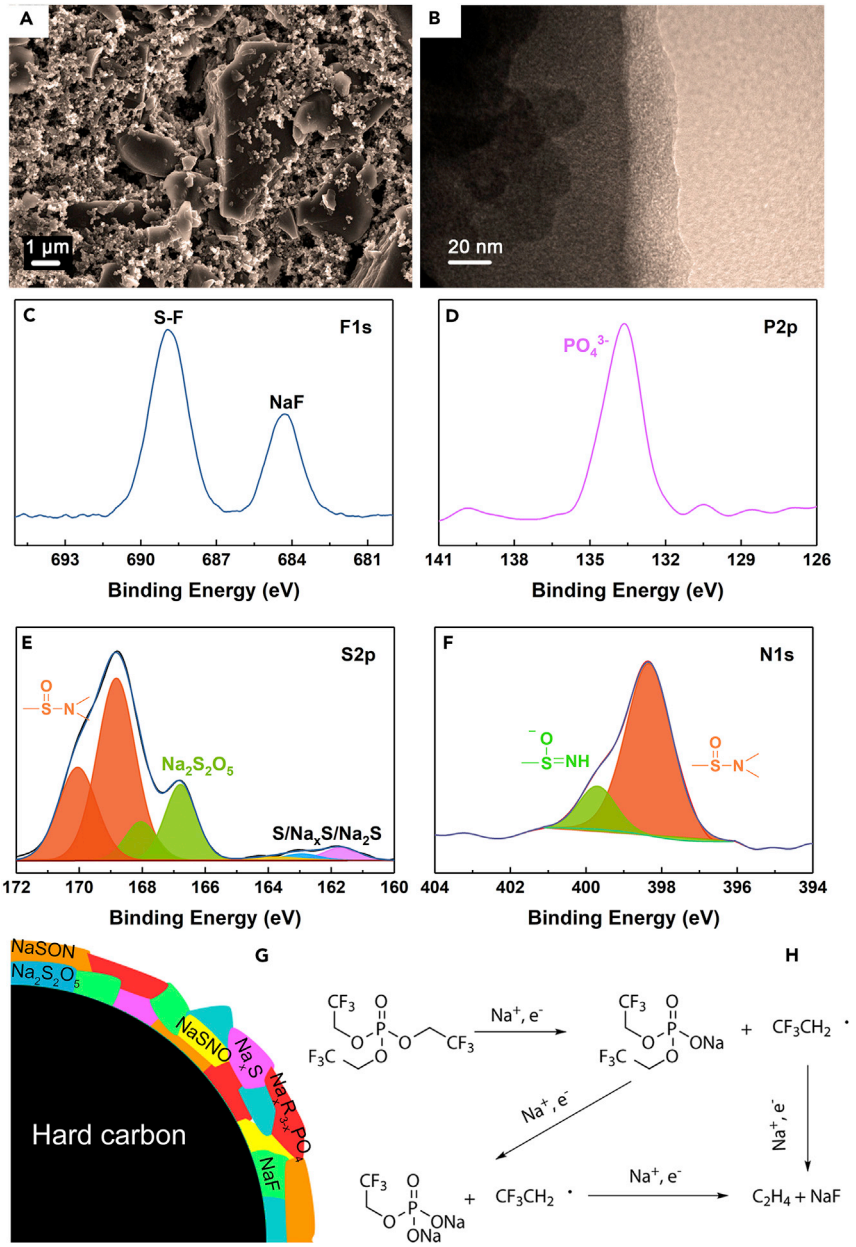

Figure 3. SEI Characterization and Formation Mechanism on a Hard Carbon Anode in TFEP-Based Electrolyte

(A and B) Scanning electron microscopic (A) and TEM (B) images of the HC anode after 10 cycles.

(C–F) XPS spectra of F 1s (C), P 2p (D), S 2p (E), and N 1s (F) spectra of the cycled HC anode.

(G) Schematic illustration of the SEI layer.

(H) Possible mechanism for the decomposition of the TFEP-derived interlayer.

See also Figures S5 and S6.

159.7, 94.5, 45.0, and 21.2 mAh g^{-1} are attained at 20, 50, 100, 200, 500, and 1,000 mA g^{-1}, respectively (Figure 4B), which are very close to those of the Na/HC half-cell. Moreover, the HC/NVP full cell exhibits a high cycling CE of above 99.5% and a high capacity retention of 89.2% after 300 cycles at 100 mA g^{-1} (Figure 4C), demonstrating an outstanding cycling durability. The energy/power densities of the full cell based on the entire mass of both electrode materials were also calculated, as shown in Figure S8. The full cell can deliver a high energy density of 143.7 Wh kg^{-1} at a power density of 13.37 W kg^{-1} and an energy density of 11.2 Wh kg^{-1} at a high power density of 571.5 W kg^{-1}, which are comparable to, or better

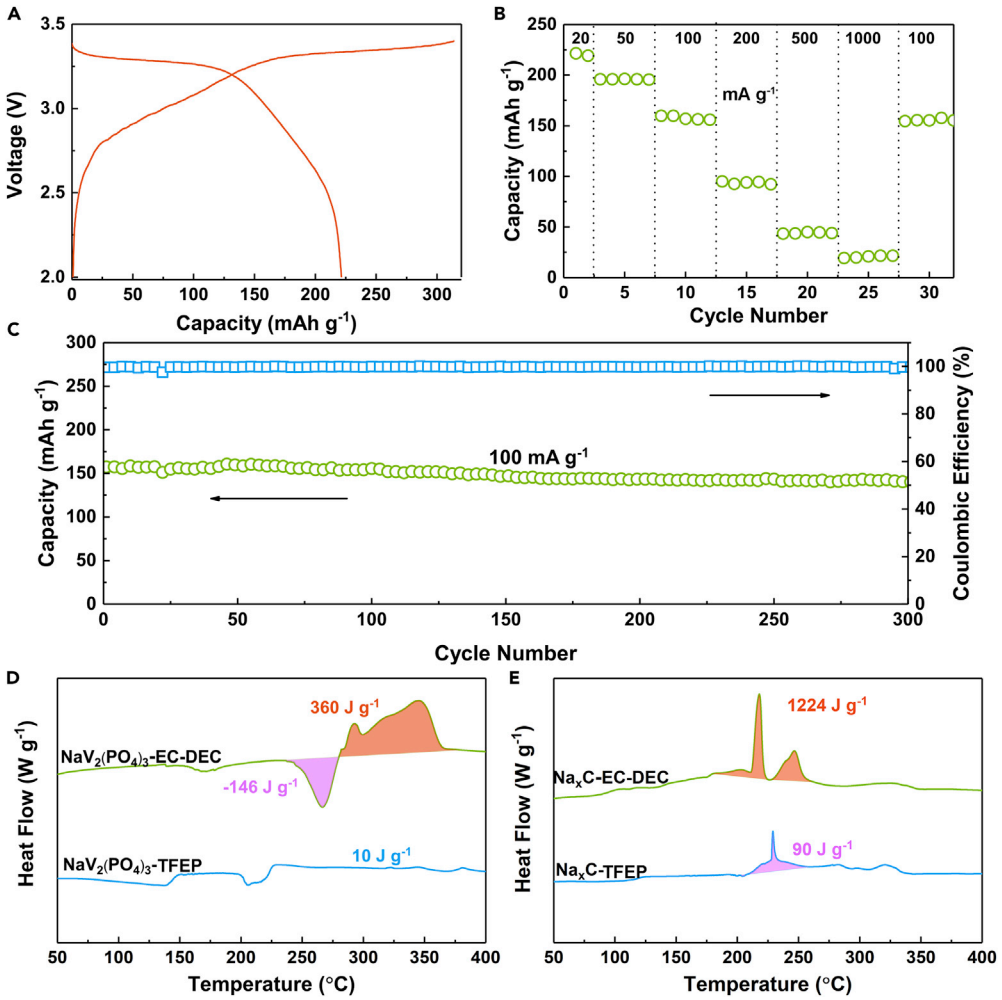

Figure 4. Electrochemical Performance and Thermal Stability of the HC/NVP Full Cell Using a 0.9 M NaFSI-TFEP Electrolyte

(A) Initial charge/discharge profile at 20 mA g^{-1} (based on HC anode).

(B) Rate capability.

(C) Cycling performance at 100 mA g^{-1}.

(D and E) DSC profiles of $NaV_2(PO_4)_3$ (D) and Na_xC (E) in carbonate and TFEP electrolytes.

See also Figures S7 and S8.

than, those reported for carbon/NVP batteries with a carbonate electrolyte (Ren et al., 2016; Feng et al., 2017).

Thermal Behavior of HC/$Na_3V_2(PO_4)_3$ Battery with 0.9 M NaFSI-TFEP

Furthermore, we examined the thermal behavior of the charged active materials ($NaV_2(PO_4)_3$ and Na_xC) in the presence of an EC-DEC electrolyte and a TFEP electrolyte via differential scanning calorimetry (DSC). As seen in Figure 4D, $NaV_2(PO_4)_3$-EC-DEC shows an endothermic peak at 265°C and an exothermic peak at 345°C, corresponding to evaporation of the carbonate electrolyte and the reaction between the electrode and electrolyte, respectively. The total heat generation is approximately 214 J g^{-1}. In contrast, the $NaV_2(PO_4)_3$-TFEP exhibits a negligible exothermic peak and heat release (~10 J g^{-1}). For the anode, Na_xC-EC-DEC displays an earlier onset temperature at ~210°C and a significantly higher heat generation of 1,224 J g^{-1} than Na_xC-TFEP (220°C and 90 J g^{-1}) (Figure 4E). The DSC results demonstrate that a TFEP-based electrolyte can not only offer flame retardancy but also significantly reduce the heat released under abusive thermal conditions, comprehensively improving battery safety.

In summary, we presented a safer SIB with a nonflammable TFEP-based electrolyte, exhibiting not only an excellent electrochemical performance but also dramatically improved safety. Under the synergistic effect of fluorine substitution and the low LUMO level of TFEP molecules, a compact and rough SEI layer is formed by the reductive decomposition of the TFEP solvent, enhancing the electrochemical compatibility to an HC anode. The stable TFEP solvent avoids the use of a high-concentration salt, making it more commercially valuable because of the high cost of salt. Moreover, the TFEP electrolyte suppresses undesirable exothermic reactions at elevated temperatures, further ensuring the safety of the SIB. This proof-of-concept study illuminates the design of advanced electrolyte systems for safe, low-cost, and high-performance SIBs for large-scale energy storage applications.

Limitations of the Study

For the currently used 0.9 M NaFSI-TFEP electrolyte, its relatively low ionic conductivity should be further enhanced to match the high-power system application requirements. It may be resolved by adding some additives to increase the entire dielectric constant of the electrolyte.

METHODS

All methods can be found in the accompanying Transparent Methods supplemental file.

SUPPLEMENTAL INFORMATION

Supplemental Information includes Transparent Methods and eight figures can be found with this article online at https://doi.org/10.1016/j.isci.2018.11.020.

ACKNOWLEDGMENTS

This work was support by the National Key Basic Research Program of China (No. 2016YFB0901500), National Natural Science Foundation of China (Nos. 21673165 and 21333007), and JCKY2016130B010.

AUTHOR CONTRIBUTIONS

Conceptualization, Y.C.; Methodology, X.J., Z.Z., and L.X.; Investigation, X.J. and X.L.; Writing - original draft, X.J.; Writing - review & editing, X.A., H.Y., and Y.C.; Funding acquisition, X.A., H.Y., and Y.C.; Resources, Y.C.; Supervision, Y.C.

DECLARATION OF INTERESTS

The authors declare no competing interests.

Received: September 21, 2018
Revised: November 4, 2018
Accepted: November 11, 2018
Published: December 21, 2018

REFERENCES

Bella, F., Colò, F., Nair, J.R., and Gerbaldi, C. (2015). Photopolymer electrolytes for sustainable, upscalable, safe, and ambient-temperature sodium-ion secondary batteries. ChemSusChem *8*, 3668–3676.

Bella, F., Muñoz-García, A.B., Meligrana, G., Lamberti, A., Destro, M., Pavone, M., and Gerbaldi, C. (2017). Unveiling the controversial mechanism of reversible Na storage in TiO_2 nanotube arrays: amorphous versus anatase TiO_2. Nano Res. *10*, 2891–2903.

Bella, F., Muñoz-García, A.B., Colò, F., Meligrana, G., Lamberti, A., Destro, M., Pavone, M., and Gerbaldi, C. (2018). Combined structural, chemometric, and electrochemical investigation of vertically aligned TiO_2 nanotubes for Na-ion batteries. ACS Omega *3*, 8440–8450.

Bommier, C., and Ji, X. (2018). Electrolytes, SEI formation, and binders: a review of nonelectrode factors for sodium-ion battery anodes. Small *14*, 1703576.

Che, H., Chen, S., Xie, Y., Wang, H., Amine, K., Liao, X.-Z., and Ma, Z.-F. (2017). Electrolyte design strategies and research progress for room-temperature sodium-ion batteries. Energy Environ. Sci. *10*, 1075–1101.

Colò, F., Bella, F., Nair, J.R., and Gerbaldi, C. (2017). Light-cured polymer electrolytes for safe, low-cost and sustainable sodium-ion batteries. J. Power Sources *365*, 293–302.

Eshetu, G.G., Grugeon, S., Kim, H., Jeong, S., Wu, L., Gachot, G., Laruelle, S., Armand, M., and Passerini, S. (2016). Comprehensive insights into the reactivity of electrolytes based on sodium ions. ChemSusChem *9*, 462–471.

Fang, Y., Yu, X.Y., and Lou, X.W. (2017). A practical high-energy cathode for sodium-ion batteries based on uniform P2-$Na_{0.7}CoO_2$ microspheres. Angew. Chem. Int. Ed. *56*, 5801–5805.

Feng, J.K., Sun, X.J., Ai, X.P., Cao, Y.L., and Yang, H.X. (2008). Dimethyl methyl phosphate: a new nonflammable electrolyte solvent for lithium-ion batteries. J. Power Sources *184*, 570–573.

Feng, P., Wang, W., Wang, K., Cheng, S., and Jiang, K. (2017). Na3V2(PO4)3/C synthesized by a facile solid-phase method assisted with agarose as a high-performance cathode for

sodium-ion batteries. J. Mater. Chem. A *5*, 10261–10268.

Feuillade, G., and Perche, P. (1975). Ion-conductive macromolecular gels and membranes for solid lithium cells. J. Appl. Electrochem. *5*, 63–69.

He, M., Lau, K.C., Ren, X., Xiao, N., McCulloch, W.D., Curtiss, L.A., and Wu, Y. (2016). Concentrated electrolyte for the sodium–oxygen battery: solvation structure and improved cycle life. Angew. Chem. Int. Ed. *55*, 15310–15314.

Iermakova, D.I., Dugas, R., Palacín, M.R., and Ponrouch, A. (2015). On the comparative stability of Li and Na metal anode interfaces in conventional alkyl carbonate electrolytes. J. Electrochem. Soc. *162*, A7060–A7066.

Jiang, X., Zeng, Z., Xiao, L., Ai, X., Yang, H., and Cao, Y. (2017). An all-phosphate and zero-strain sodium-ion battery based on $Na_3V_2(PO_4)_3$ cathode, $NaTi_2(PO_4)_3$ anode, and trimethyl phosphate electrolyte with intrinsic safety and long lifespan. ACS Appl. Mater. Interfaces *9*, 43733–43738.

Jiang, X., Liu, X., Zeng, Z., Xiao, L., Ai, X., Yang, H., and Cao, Y. (2018). A nonflammable Na^+-based dual-carbon battery with low-cost, high voltage, and long cycle life. Adv. Energy Mater. 1802176, https://doi.org/10.1002/aenm.201802176.

Kim, H., Wu, F., Lee, J.T., Nitta, N., Lin, H.T., Oschatz, M., Cho, W.I., Kaskel, S., Borodin, O., and Yushin, G. (2015). In situ formation of protective coatings on sulfur cathodes in lithium batteries with LiFSI-based organic electrolytes. Adv. Energy Mater. *5*, 1401792.

Kim, J.I., Choi, Y., Chung, K.Y., and Park, J.H. (2017). A structurable gel-polymer electrolyte for sodium ion batteries. Adv. Funct. Mater. *27*, 1701768.

Komaba, S., Ishikawa, T., Yabuuchi, N., Murata, W., Ito, A., and Ohsawa, Y. (2011). Fluorinated ethylene carbonate as electrolyte additive for rechargeable Na batteries. ACS Appl. Mater. Interfaces *3*, 4165–4168.

Lee, Y., Lee, J., Lee, J., Kim, K., Cha, A., Kang, S., Wi, T., Kang, S.J., Lee, H.-W., and Choi, N.-S. (2018). Fluoroethylene carbonate-based electrolyte with 1 M sodium bis(fluorosulfonyl) imide enables high-performance sodium metal electrodes. ACS Appl. Mater. Interfaces *10*, 15270–15280.

Li, X., Qian, K., He, Y.-B., Liu, C., An, D., Li, Y., Zhou, D., Lin, Z., Li, B., Yang, Q.-H., and Kang, F. (2017). A dual-functional gel-polymer electrolyte for lithium ion batteries with superior rate and safety performances. J. Mater. Chem. A *5*, 18888–18895.

Liu, J., Song, X., Zhou, L., Wang, S., Song, W., Liu, W., Long, H., Zhou, L., Wu, H., Feng, C., and Guo, Z. (2018a). Fluorinated phosphazene derivative-a promising electrolyte additive for high voltage lithium ion batteries: from electrochemical performance to corrosion mechanism. Nano Energy *46*, 404–414.

Liu, X., Jiang, X., Zeng, Z., Ai, X., Yang, H., Zhong, F., Xia, Y., and Cao, Y. (2018b). High capacity and cycle-stable hard carbon anode for nonflammable sodium-ion batteries. ACS Appl. Mater. Interfaces *10*, 38141–38150.

Matsumoto, K., Inoue, K., and Utsugi, K. (2015). A highly safe battery with a non-flammable triethyl-phosphate-based electrolyte. J. Power Sources *273*, 954–958.

Mogensen, R., Brandell, D., and Younesi, R. (2016). Solubility of the solid electrolyte interphase (SEI) in sodium ion batteries. ACS Energy Lett. *1*, 1173–1178.

Okuno, Y., Ushirogata, K., Sodeyama, K., and Tateyama, Y. (2016). Decomposition of the fluoroethylene carbonate additive and the glue effect of lithium fluoride products for the solid electrolyte interphase: an ab initio study. Phys. Chem. Chem. Phys. *18*, 8643–8653.

Patra, J., Huang, H.-T., Xue, W., Wang, C., Helal, A.S., Li, J., and Chang, J.-K. (2019). Moderately concentrated electrolyte improves solid–electrolyte interphase and sodium storage performance of hard carbon. Energy Storage Mater. *16*, 146–154.

Philippe, B., Dedryvère, R., Gorgoi, M., Rensmo, H., Gonbeau, D., and Edström, K. (2013). Improved performances of nanosilicon electrodes using the salt LiFSI: a photoelectron spectroscopy study. J. Am. Chem. Soc. *135*, 9829–9842.

Qi, L., Daobin, M., Borong, W., Lei, W., Liang, G., and Feng, W. (2017). Density functional theory research into the reduction mechanism for the solvent/additive in a sodium-ion battery. ChemSusChem *10*, 786–796.

Qiu, S., Xiao, L., Sushko, M.L., Han, K.S., Shao, Y., Yan, M., Liang, X., Mai, L., Feng, J., Cao, Y., et al. (2017). Manipulating adsorption-insertion mechanisms in nanostructured carbon materials for high-efficiency sodium ion storage. Adv. Energy Mater. *7*, 1700403.

Rao, M.C., Koutavarapu, R., and Kumar, K.V. (2019). Structural and electrochemical properties of ZrO_2 doped PVP-Na^+ based nanocomposite polymer films. Mater. Sci. Semicond. Process. *89*, 41–50.

Ren, W., Yao, X., Niu, C., Zheng, Z., Zhao, K., An, Q., Wei, Q., Yan, M., Zhang, L., and Mai, L. (2016). Cathodic polarization suppressed sodium-ion full cell with a 3.3 V high-voltage. Nano Energy *28*, 216–223.

Shinichi, K., Wataru, M., Toru, I., Naoaki, Y., Tomoaki, O., Tetsuri, N., Atsushi, O., Kazuma, G., and Kazuya, F. (2011). Electrochemical Na insertion and solid electrolyte interphase for hard-carbon electrodes and application to Na-ion batteries. Adv. Funct. Mater. *21*, 3859–3867.

Sogawa, M., Todorov, Y.M., Hirayama, D., Mimura, H., Yoshimoto, N., Morita, M., and Fujii, K. (2017). Role of solvent bulkiness on lithium-ion solvation in fluorinated alkyl phosphate-based electrolytes: structural study for designing nonflammable lithium-ion batteries. J. Phys. Chem. C *121*, 19112–19119.

Song, J., Xiao, B., Li, Y., Xu, K., and Li, X. (2018). Interphases in sodium-ion batteries. Adv. Energy Mater. *8*, 1703082.

Wang, J., Yamada, Y., Sodeyama, K., Watanabe, E., Takada, K., Tateyama, Y., and Yamada, A. (2018). Fire-extinguishing organic electrolytes for safe batteries. Nat. Energy *3*, 22–29.

Westman, K., Dugas, R., Jankowski, P., Wieczorek, W., Gachot, G., Morcrette, M., Irisarri, E., Ponrouch, A., Palacín, M.R., Tarascon, J.M., and Johansson, P. (2018). Diglyme based electrolytes for sodium-ion batteries. ACS Appl. Energy Mater. *1*, 2671–2680.

Wu, X., Qi, Y., Hong, J.J., Li, Z., Hernandez, A.S., and Ji, X. (2017). Rocking-chair ammonium-ion battery: a highly reversible aqueous energy storage system. Angew. Chem. Int. Ed. *129*, 13206–13210.

Xia, L., Yu, L., Hu, D., and Chen, G.Z. (2017). Electrolytes for electrochemical energy storage. Mater. Chem. Front. *1*, 584–618.

Xiang, C., Xin, S., Bo, L., Hong-Jie, P., Xin-Bing, C., Bo-Quan, L., Xue-Qiang, Z., Jia-Qi, H., and Qiang, Z. (2018). Ion-solvent complexes promote gas evolution from electrolytes on a sodium metal anode. Angew. Chem. Int. Ed. *57*, 734–737.

Xiao, L., Lu, H., Fang, Y., Sushko, M.L., Cao, Y., Ai, X., Yang, H., and Liu, J. (2018). Low-defect and low-porosity hard carbon with high coulombic efficiency and high capacity for practical sodium ion battery anode. Adv. Energy Mater. *8*, 1703238.

Xu, K. (2014). Electrolytes and interphases in Li-ion batteries and beyond. Chem. Rev. *114*, 11503–11618.

Xu, K., Ding, M.S., Zhang, S., Allen, J.L., and Jow, T.R. (2002). An attempt to formulate nonflammable lithium ion electrolytes with alkyl phosphates and phosphazenes. J. Electrochem. Soc. *149*, A622–A626.

Xu, K., Zhang, S., Allen, J.L., and Jow, T.R. (2003). Evaluation of fluorinated alkyl phosphates as flame retardants in electrolytes for Li-ion batteries: II. Performance in cell. J. Electrochem. Soc. *150*, A170–A175.

Xu, Z., Wang, J., Yang, J., Miao, X., Chen, R., Qian, J., and Miao, R. (2016). Enhanced performance of a lithium-sulfur battery using a carbonate-based electrolyte. Angew. Chem. Int. Ed. *55*, 10372–10375.

Yamada, Y., and Yamada, A. (2015). Review—superconcentrated electrolytes for lithium batteries. J. Electrochem. Soc. *162*, A2406–A2423.

Yamada, Y., Furukawa, K., Sodeyama, K., Kikuchi, K., Yaegashi, M., Tateyama, Y., and Yamada, A. (2014). Unusual stability of acetonitrile-based superconcentrated electrolytes for fast-charging lithium-ion batteries. J. Am. Chem. Soc. *136*, 5039–5046.

Yang, H., Li, Q., Guo, C., Naveed, A., Yang, J., Nuli, Y., and Wang, J. (2018). Safer lithium-sulfur

battery based on nonflammable electrolyte with sulfur composite cathode. Chem. Commun. (Camb.) *54*, 4132–4135.

Zeng, Z., Jiang, X., Li, R., Yuan, D., Ai, X., Yang, H., and Cao, Y. (2016). A safer sodium-ion battery based on nonflammable organic phosphate electrolyte. Adv. Sci. *3*, 1600066.

Zeng, Z., Murugesan, V., Han, K.S., Jiang, X., Cao, Y., Xiao, L., Ai, X., Yang, H., Zhang, J.-G., Sushko, M.L., and Liu, J. (2018). Improving compatibility of nonflammable electrolytes with high salt-to-solvent ratios in Li-ion and Li-metal batteries. Nat. Energy *3*, 674–681.

Zhang, J., Wen, H., Yue, L., Chai, J., Ma, J., Hu, P., Ding, G., Wang, Q., Liu, Z., Cui, G., and Chen, L. (2017). In situ formation of polysulfonamide supported poly(ethylene glycol) divinyl ether based polymer electrolyte toward monolithic sodium ion batteries. Small *13*, 1601530.

Zhao, J., Zhao, L., Chihara, K., Okada, S., Yamaki, J.-i., Matsumoto, S., Kuze, S., and Nakane, K. (2013). Electrochemical and thermal properties of hard carbon-type anodes for Na-ion batteries. J. Power Sources *244*, 752–757.

Zhao, W., Ji, Y., Zhang, Z., Lin, M., Wu, Z., Zheng, X., Li, Q., and Yang, Y. (2017). Recent advances in the research of functional electrolyte additives for lithium-ion batteries. Curr. Opin. Electrochem. *6*, 84–91.

Zheng, J., Zhao, Y., Feng, X., Chen, W., and Zhao, Y. (2018). Novel safer phosphonate-based gel polymer electrolytes for sodium-ion batteries with excellent cycling performance. J. Mater. Chem. A *6*, 6559–6564.

ISCI, Volume *10*

Supplemental Information

A Bifunctional Fluorophosphate Electrolyte for Safer Sodium-Ion Batteries

Xiaoyu Jiang, Xingwei Liu, Ziqi Zeng, Lifen Xiao, Xinping Ai, Hanxi Yang, and Yuliang Cao

SUPPLEMENTAL FIGURES

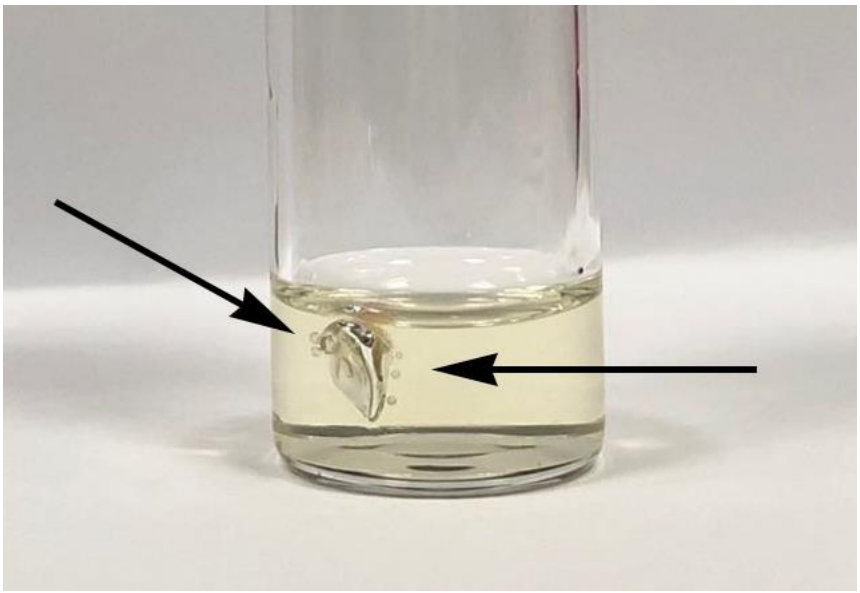

Figure S1. Photograph of Na metal in TEP solvent for one day, related to Figure 1.

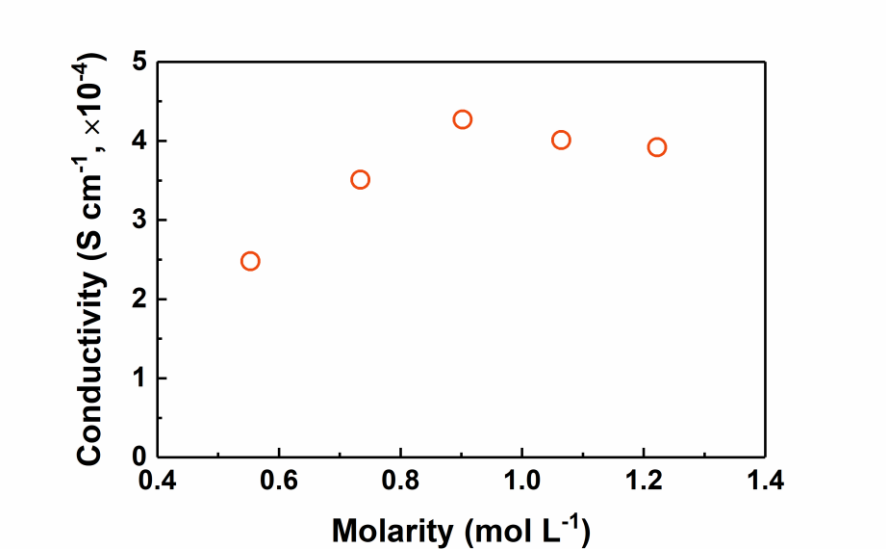

Figure S2. Molarity dependence of the ionic conductivity of NaFSI-TFEP electrolyte at room temperature, related to Figure 2.

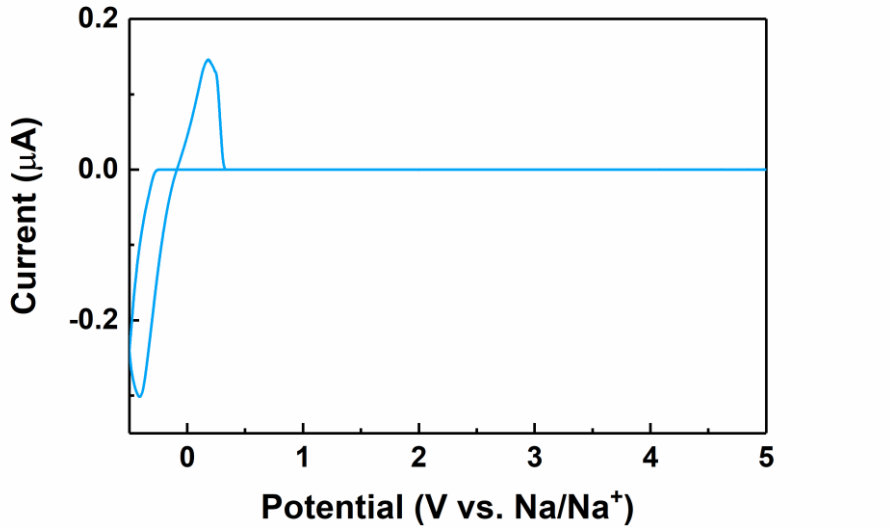

Figure S3. CV curve of a Pt microelectrode in 0.9 M NaFSI-TFEP electrolyte at 10 mV s^{-1}, related to Figure 2.

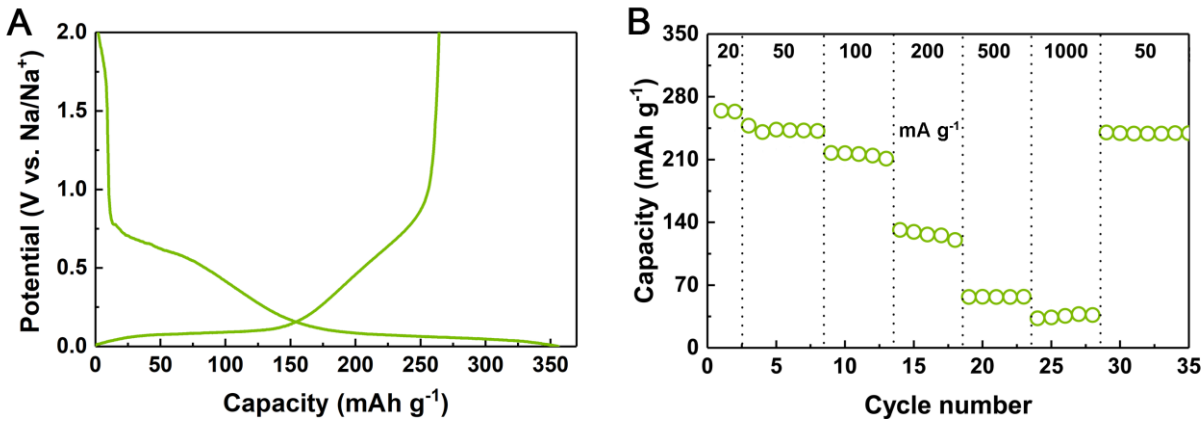

Figure S4. Electrochemical performances of HC anode in 1 M $NaClO_4$-EC/DEC electrolyte, related to Figure 2.

(A) Initial charge/discharge profile at 20 mA g^{-1}.

(B) Rate capability.

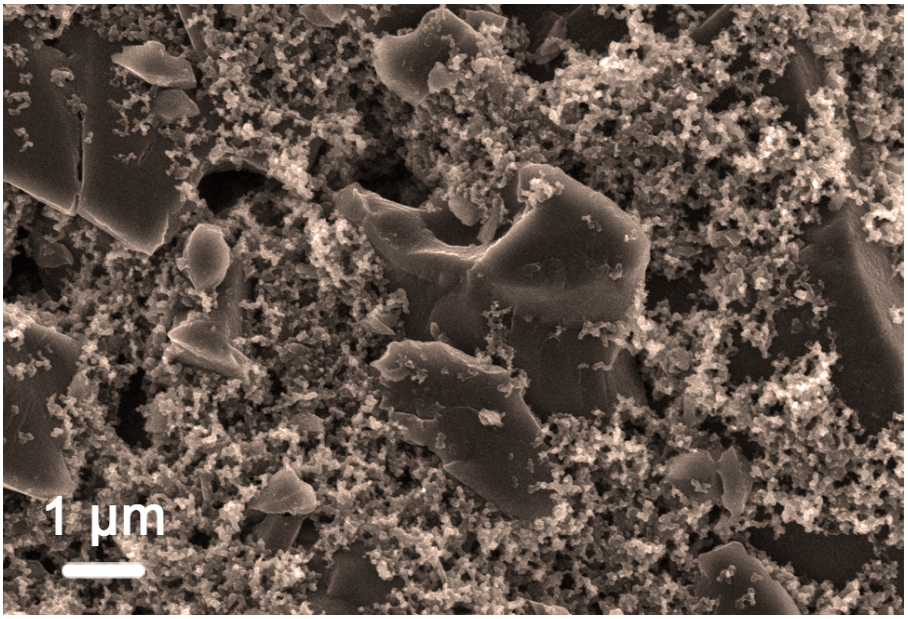

Figure S5. SEM image of the pristine HC anode, related to Figure 3.

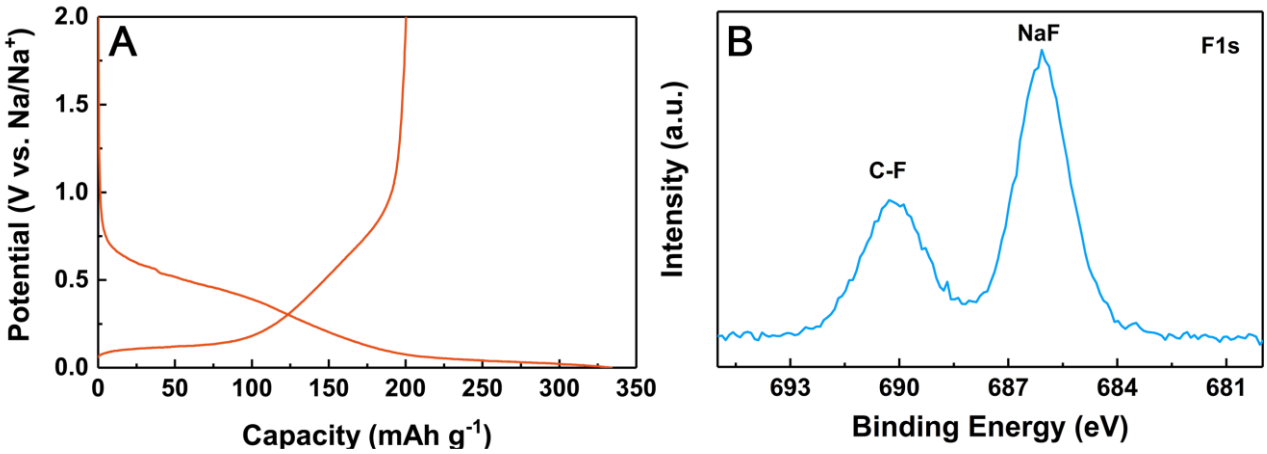

Figure S6. Electrochemical performances and XPS Spectra of HC anode in the $NaClO_4$-TFEP electrolyte, related to Figure 3.

(A) Initial charge/discharge curve at 20 mA g^{-1}.

(B) F1s spectrum.

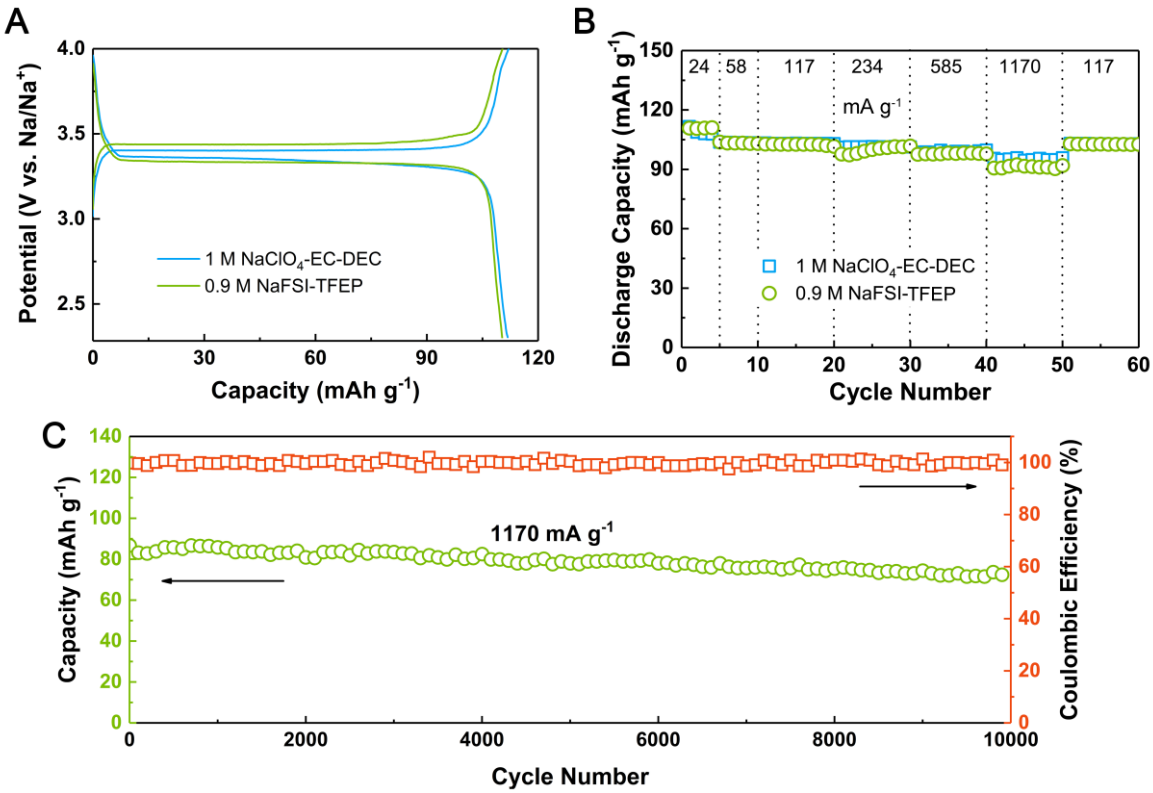

Figure S7. Electrochemical performances of NVP cathode, related to Figure 4.

(A) Initial charge-discharge profile of NVP in 0.9 M NaFSI-TFEP and 1 M $NaClO_4$-EC/DEC electrolyte at 24 mA g^{-1}.

(B) Rate capability in 0.9 M NaFSI-TFEP and 1 M $NaClO_4$-EC/DEC electrolyte.

(C) Cycling performance in 0.9 M NaFSI-TFEP electrolyte.

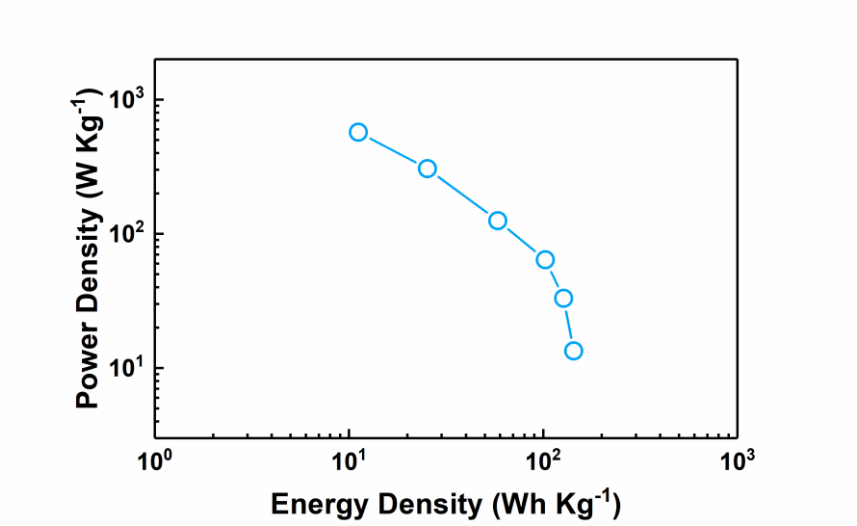

Figure S8. Ragone plot of rate capability for the HC/NVP full cell using 0.9 M NaFSI-TFEP electrolyte, related to Figure 4.

Transparent Methods

Synthesis of tris(2,2,2-trifluoroethyl) phosphate (TFEP). 0.2 mol of trifluoroethanol, 0.06 mol of phosphorus oxychloride and 0.01 mol of LiCl were mixed together and refluxed at 90°C for 8 hr. Then, the mixture was washed with aqueous $NaHCO_3$ to neutral, followed by washing with distilled water three times and dried over CaH_2. The resulting TFEP was isolated by vacuum distillation and gave a yield of 70%. The chemical structure was determined by nuclear magnetic resonance (NMR, 400 MHz, $CDCl_3$), as shown below: ^{1}H NMR: 4.43 (dq, 6H, —OC**H$_2$**CF_3), ^{13}C NMR: 122.0 (dq, 3C, —OCH_2**C**F_3), 64.32 (dq, 3C, —O**C**H_2CF_3), ^{31}P NMR: −2.77 (s, 1P, —**P**=O), ^{19}F NMR: −75.44 (t, 9F, —OCH_2C**F$_3$**).

Synthesis of carbon-coated $Na_3V_2(PO_4)_3$ (NVP). 0.04 mol of oxalic acid and 0.01 mol of V_2O_5 were dispersed in 100 mL of water under magnetic stirring at 80°C. Then, 0.03 mol of NaH_2PO_4 and 1.15 g of glucose were added into the solution and stirred for 1 hr. The as-prepared solution was injected into the spray dryer (SD-1500, Triowin Co., Ltd, China) at a rate of 300 mL h^{-1} and then converted into precursor particle with an inlet temperature of 200°C and an outlet temperature of 110°C. The precursor was calcined under an Ar atmosphere for 8 hr with a heating rate of 2°C min^{-1} to produce carbon-coated NVP.

***Preparation of electrolytes*.** Sodium bis(fluorosulfonyl)imide (NaFSI, 98%, TCI) and $NaClO_4$ (Sigma-Aldrich, 98%) were dissolved in TFEP in the molarities of 0.9 mol L^{-1} and 0.3 mol L^{-1} (nearly saturated), respectively. For comparison, a conventional carbonate electrolyte of 1 M $NaClO_4$ in EC-DEC (1:1 by volume) was prepared.

***Fabrication of electrodes*.** The cathode was prepared by applying the N-methyl pyrrolidone (NMP) paste composed of 70 wt % NVP, 20 wt % Super-P carbon and 10 wt % poly(vinyl difluoride) (PVDF) onto an Al foil. The average mass loading of the active material was approximately 3 mg cm^{-2}. The

anode was prepared by casting the aqueous slurry consisting of 80 wt % hard carbon (LBV-10010, Sumitomo Bakelite Co., Ltd.), 10 wt % Super-P carbon and 10 wt % polyacrylic acid (PAA). The average mass loading of the active material was approximately 1.8 mg cm^{-2}. Both cathode and anode were dried under vacuum at 100°C overnight before use.

***Characterization*.** SEM and TEM were conducted using a field-emission scanning electron microscope (ZEISS Merlin Compact VP, Germany) and a transmission electron microscope (JEM-2100, Japan), respectively. XPS was recorded with a Thermo Fisher ESCALAB 250Xi using a monochromic Al Kα X-ray source. Thermal analysis of the electrodes and electrolytes was conducted using differential scanning calorimetry (Q200, TA, America) at a heating rate of 10°C min^{-1} from 50 to 400°C. For postmortem SEM TEM, and XPS measurements of the electrode, the half cells were disassembled in an Ar-filled glove box after 10 cycles at 20 mA g^{-1} and the electrodes were rinsed by dimethyl carbonate three times and dried under vacuum for 1 hr.

***Electrochemical measurements*.** The ionic conductivity of the electrolytes was measured via a conductivity meter (DDS-307, Leici, China) at 25°C. Standard CR2016 coin cells were assembled in an Ar-filled glove box (O_2 and H_2O < 0.5 ppm). The hand-made sodium plate was used as both counter and reference electrode in half cells. The glass fiber membrane (GF/D, Whatman) is used as a separator and the electrolyte amount is 50 µL per cell. CV measurements were conducted with an electrochemical workstation (Gamry Ref 3000, America) at the scan rate of 10 and 0.1 mV s^{-1} for Pt microelectrode and hard carbon anode, respectively. Galvanostatic charge-discharge studies were conducted on a battery cycler (CT2001D, LAND Electronics Co., China) between 0-2 V and 2.3-4 V for HC anode and NVP cathode, respectively. The ratio of the cathode mass to anode mass was set to 3.7:1 in the full cell and the tested voltage range for the full cell was 2-3.4 V.